J. Synchrotron Rad. (2000). **7**, 34–39

Mapping of a particular element using an absorption edge with an X-ray fluorescence imaging microscope

Kimitake Yamamoto,* Norio Watanabe, Akihisa Takeuchi, Hidekazu Takano, Tatsuya Aota, Masanori Fukuda and Sadao Aoki

Institute of Applied Physics, University of Tsukuba, 1-1-1 Tennnoudai, Tsukuba, Ibaraki 305-8573, Japan. E-mail: yamamoto@aokilab.bk.tsukuba.ac.jp

(*Received 8 August 1999; accepted 4 November 1999*)

An X-ray fluorescence imaging microscope with a Wolter-type objective mirror (magnification: 13) has been constructed at beamline 39XU of SPring-8. Monochromatic X-rays ($\Delta E/E \simeq 10^{-4}$) in the energy range 6–10 keV were used for X-ray fluorescence excitation of the specimens. Using two monochromatic X-rays above and below the absorption edge of a particular element, a two-dimensional image of the element could be obtained. As a result, two-dimensional element mapping of the test specimens (Cu, Co, Ni, Fe and Ti wires) and constituent minerals (Fe, Mn and Ti) of a rock specimen (a piemontite-quartz schist) became possible.

Keywords: imaging; X-ray fluorescence; microscopes; Wolter-type mirrors.

1. Introduction

X-ray fluorescence microanalysis has been rapidly developed by using X-ray microprobes. Typical microprobes are Kirkpatrick–Baez mirrors (Eng *et al.*, 1998), capillary tubes (Bilderback *et al.*, 1994), Fresnel zone plates (Yun *et al.*, 1999; Suzuki *et al.*, 1997), Bragg–Fresnel lenses (Snigireva *et al.*, 1997), Wolter mirrors (Aoki *et al.*, 1997) and so on. They are usually used as focusing elements for scanning X-ray fluorescence microscopes (SXFM), which are very convenient for mapping a particular element. While an SXFM is a powerful tool for obtaining a two-dimensional element image and requires a very accurate position control and a relatively long measuring time, an imaging X-ray fluorescence microscope (IXFM) needs only a moderate position control system and can record an image in a reasonably short time. This will make it possible to observe the three-dimensional distribution of a trace element in a bulk sample or in a liquid state.

In a previous paper we demonstrated that X-ray fluorescence could be successfully imaged with a Wolter-type mirror (Aoki *et al.*, 1998). As the mirror has no chromatic aberration, all the X-rays above the critical wavelength can be imaged simultaneously. In order to obtain an image of a particular element, an absorption edge of the element concerned can be utilized. Very bright synchrotron radiation is suitable for this kind of imaging.

In this paper we show the X-ray optical system constructed at beamline 39XU of SPring-8, and then X-ray fluorescence images of metal wires are given. Application of the imaging to a rock specimen is also given.

2. Optical systems

We have constructed an X-ray fluorescence imaging microscope by using a Wolter mirror at SPring-8. A schematic diagram of the experimental arrangement at beamline 39XU is shown in Fig. 1. The incident X-ray path

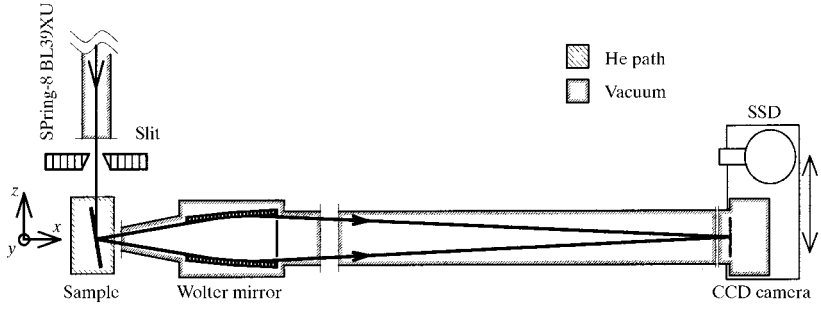

Figure 1
Schematic diagram of the experimental arrangement.

between the upstream end of the experimental hutch and the slit was evacuated. To reduce the absorption of X-rays in the air, the sample chamber was filled with He gas. The geometrical parameters of the Wolter mirror are shown in Fig. 2. The optical axis of the Wolter mirror was set normal to the incident beam, which reduced the elastic scattering from specimens and improved the signal/background ratio. The X-ray fluorescence path between the specimen and the detector was also evacuated. X-rays from 4 keV to 12 keV can be imaged with this optical system.

The area detector was an X-ray sensitive charge-coupled device (CCD) camera (HAMAMATSU, TI, TC-215). The number of pixels was 1000 × 1018 and each pixel area was 12 μm × 12 μm. As the magnification of this mirror was 13, the unit area at the sample plane was calculated to be 0.96 μm × 0.96 μm. The detector was cooled by a Peltier cooler below 253 K to reduce the dark current. An energy-dispersive detector was used, in this case a Ge solid-state detector (SSD). The quasi-monochromatic undulator radiation was monochromated with a rotated-inclined double-crystal monochromator equipped with Si(111) crystals (Kitamura, 1994). The energy bandwidth ($\Delta E/E$) was $\sim 1 \times 10^{-4}$ in our experiment. Any residual higher-order undulator radiation was eliminated by a Pt-coated plane mirror.

3. Experimental results

3.1. *X-ray fluorescence image of particular elements*

Five kinds of metallic wire (Cu, Ni, Co and Ti wires of diameter 50 μm; Fe wire of diameter 100 μm) were used to evaluate the performance of the microscope. X-ray fluorescence images of the wires were taken by changing the excitation energy of the incident X-ray. Figs. 3(*a*)–3(*e*) show the X-ray fluorescence images of the five wires taken using different incidence X-ray energies. Fig. 3(*a*) shows the X-ray fluorescence image of the wires and its spectrum obtained on the image plane with a Ge SSD at an excitation energy of 10 keV. The exposure time was 2 min. Figs. 3(*b*)–3(*e*) show the X-ray fluorescence images and their spectra, which were obtained with excitation energies 10 eV below the absorption edges of the Cu, Ni, Co and Fe elements. The exposure time of the X-ray fluorescence images of Cu and Ni was 2 min (Figs. 3*b* and 3*c*, respectively), of Co 3 min (Fig. 3*d*) and of Fe 12 min (Fig. 3*e*). It took 100 s for each measurement of the spectra. Figs. 3(*f*)–3(*i*) show the X-ray fluorescence images of the particular element and their spectra which were obtained by subtracting the adjacent data. There were negative values in their spectra because the influence of the fluctuation of the background was not considered in this subtraction. Although the subtracted image of Cu includes some background, images of Ni, Co and Fe were well resolved. The results show that the selective excitation of a particular element can be made by using an absorption edge. Fig. 3(*j*) shows the visible-light image of the wires after exposure. The Fe wire was badly damaged; the reason behind this is under investigation.

The spatial resolution was estimated by using a copper sheet grid (#500). Fig. 4 shows the X-ray fluorescence image of the grid and its intensity profile. From the profile, the spatial resolution was estimated to be ~10 μm.

3.2. *Application to a rock specimen (a piemontite-quartz schist)*

In order to show the practical applicability of the microscope, a piemontite-quartz schist was analyzed.

Piemontite-quartz schists are found in the greenschist facies metamorphic belt of Japan. The chemistry of its constituent minerals is important for understanding the metamorphic conditions in the orogenic area. A piemontite-quartz schist contains piemontite, $Ca_2(Mn^{3+},Fe^{3+},Al)_2$-$AlO{\cdot}OH[Si_2O_7][SiO_4]$; hematite, ($\alpha$-$Fe_2O_3$; titanite, $CaTi$-$[SiO_4](O,OH,F)$; muscovite, $Ka_2Al_4[Si_6Al_2O_{20}](OH,F)_4$; quartz, SiO_2; apatite, $Ca_5(PO_4)_3$ (Deer *et al.*, 1975). Because the tunable range of the undulator is above 5 keV, excitation energies below 5 keV were not selected. Also, because the fluorescent yield of the light elements is much lower than that of the heavy elements, the excitation energies of the heavy elements (Fe, Mn and Ti) are selected. Figs. 5(*a*) and 5(*b*) show the X-ray fluorescence images and their spectra of the piemontite-quartz schist, which were obtained with an excitation energy 20 eV above the absorption edges of the Fe and Mn elements. Fig. 5(*c*) shows the X-ray fluorescence image and its spectrum, which were obtained with an excitation energy 20 eV below

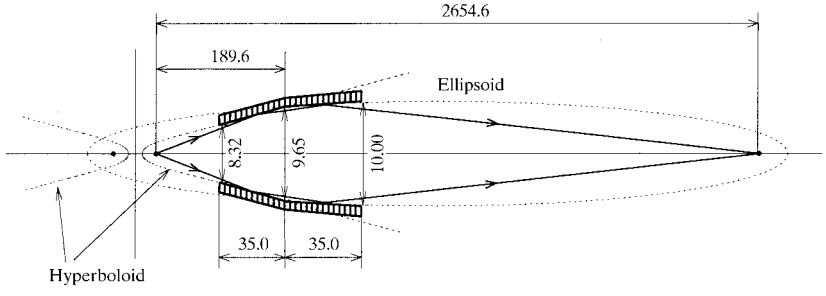

Figure 2
Parameters of the Wolter-type mirror. Average grazing angle: 7 mrad. Material: Pyrex glass. Mirror surface: Pt-coated. Magnification: 13. All dimensions are in mm.

the absorption edge of the Mn element. The exposure time of the X-ray fluorescence images is 10 min and the measurement time of the spectra is 300 s. Figs. 5(*d*) and 5(*e*) show the X-ray fluorescence images and their spectra, which were obtained by subtracting the data taken above and below the absorption edges of the Fe and Mn elements, respectively. Fig. 5(*f*) shows the visible-light image of the piemontite-quartz schist. The four regions in this sample correspond to (1) piemontite, (2) hematite, (3) titanite and (4) a matrix area consistency of quartz, plagioclase,

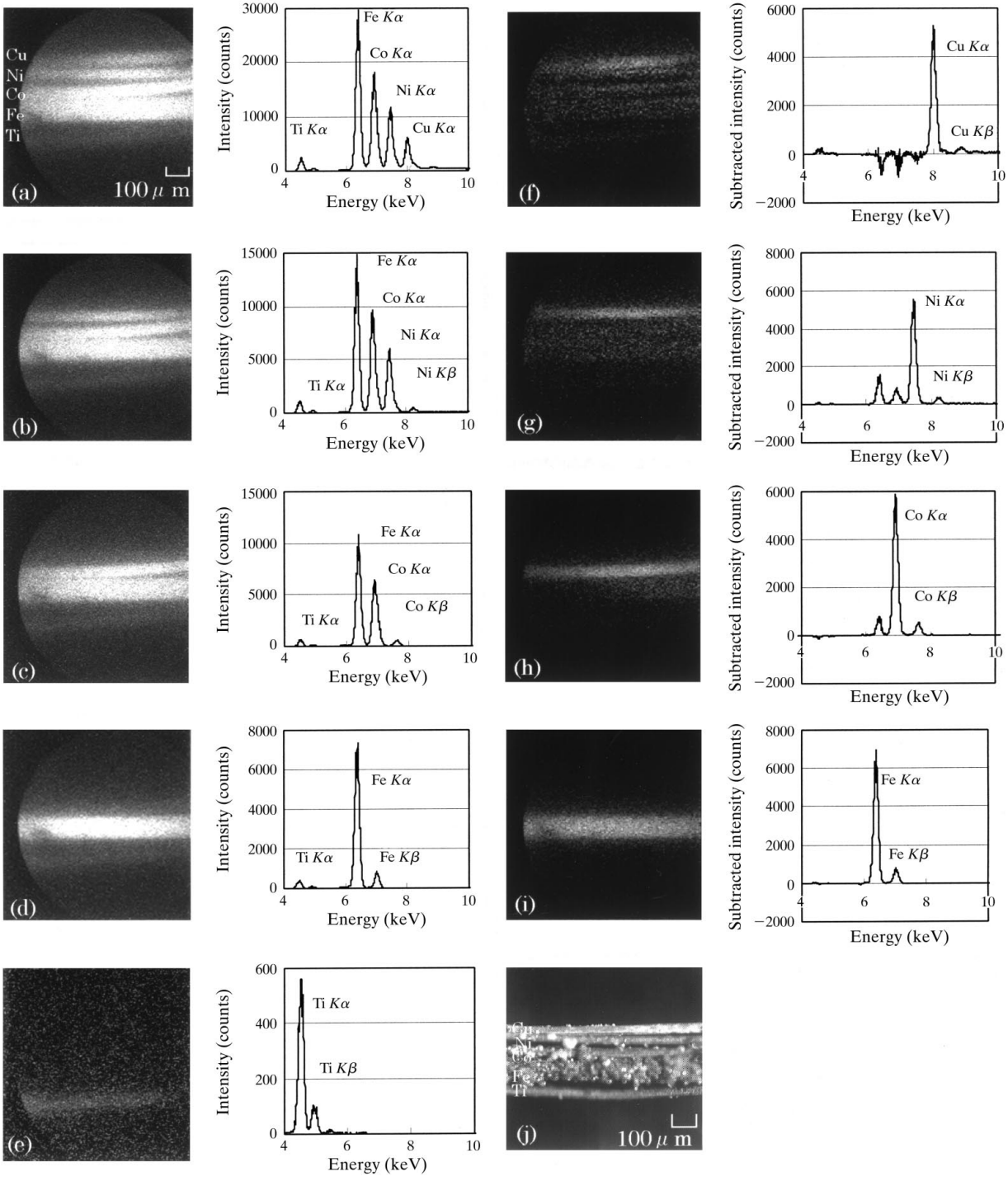

Figure 3
The X-ray fluorescence images of five kinds of metallic wires and their spectra at an excitation energy of (*a*) 10 keV, (*b*) 8.970 keV (10 eV below the absorption edge of Cu), (*c*) 8.323 keV (10 eV below the absorption edge of Ni), (*d*) 7.699 keV (10 eV below the absorption edge of Co) and (*e*) 7.102 keV (10 eV below the absorption edge of Fe). The X-ray fluorescence images and their spectra, which were obtained by subtracting the data taken above and below the absorption edges of (*f*) the Cu *K*-edge (8.980 keV), (*g*) the Ni *K*-edge (8.333 keV), (*h*) the Co *K*-edge (7.709 keV) and (*i*) the Fe *K*-edge (7.112 keV). (*j*) A visible-light image after exposure.

muscovite and apatite. Trace-elemental images of Fe, Mn and Ti seem to be attributed to hematite, piemontite and titanite, respectively. By combining the image with the spectrum, a two-dimensional trace-elemental analysis (Fe, Mn and Ti) of the piemontite-quartz schist becomes possible.

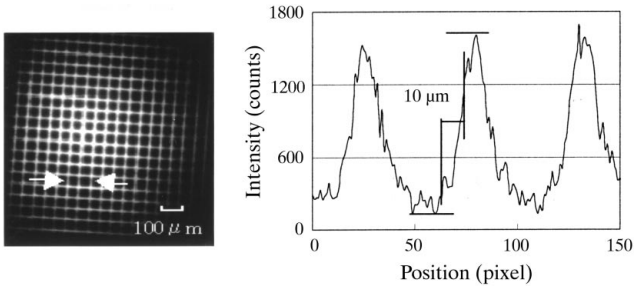

Figure 4
X-ray fluorescence image of a copper grid (#500) and its intensity profile.

4. Discussion

In order to examine the experimental results it is necessary to calculate the X-ray fluorescence intensity of the image. In this section the estimation of the Fe $K\alpha$ fluorescence count rate is described, and then the experimental results are discussed.

First, the Fe $K\alpha$ fluorescence X-ray intensity from the 100 μm-diameter Fe wire is calculated at an incident X-ray energy of 7.122 keV, as follows. BL39XU is equipped with an in-vacuum-type linear undulator which comprises 140 sets of permanent magnets whose period is 32 mm (Kitamura, 1994). A brilliance of 4.0×10^{18} photons s^{-1} $mrad^{-2}$ mm^{-2} (0.1% bandwidth)$^{-1}$ is calculated at a 20 mA storage-ring current (Kitamura, 1998). The size of the source is $2.35^2\sigma_x\sigma_y$, where σ_x and σ_y are the standard deviations of the electron beam size at the x and y axes, respectively. At an excitation energy of 7.122 keV, σ_x and σ_y are 0.394 mm and 0.0272 mm, respectively (Kitamura, 1998). Therefore the brightness is 2.36×10^{17} photons s^{-1} $mrad^{-2}$ (0.1% bandwidth)$^{-1}$. A rotated-inclined double-

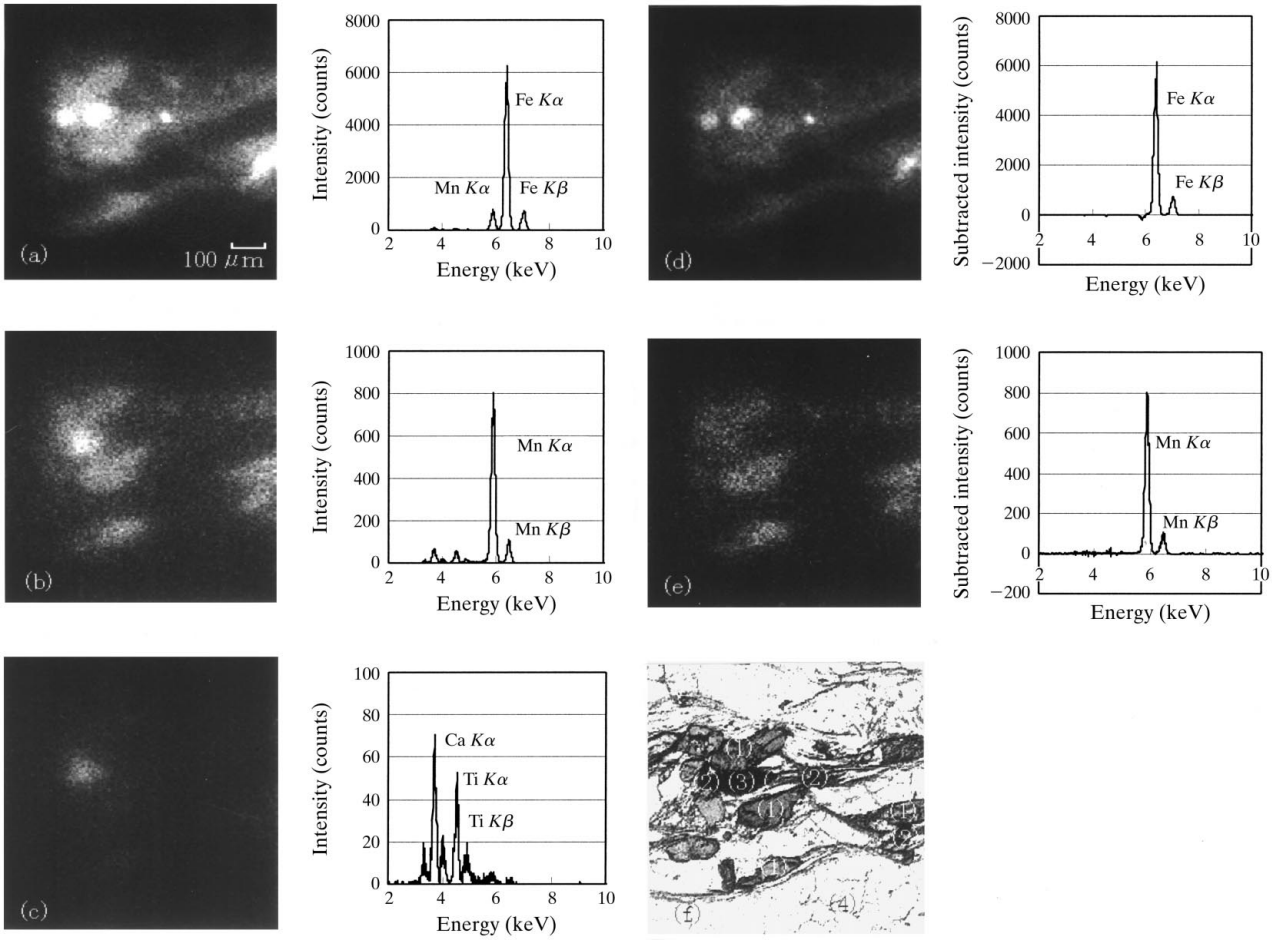

Figure 5
X-ray fluorescence images and spectra of the piemontite-quartz schist at an excitation energy of (*a*) 7.132 keV (20 eV above the absorption edge of Fe), (*b*) 6.557 keV (20 eV above the absorption edge of Mn), (*c*) 6.517 keV (20 eV below the absorption edge of Mn). X-ray fluorescence images and their spectra, which were obtained by subtracting the data taken above and below the absorption edges of (*d*) the Fe *K*-edge (7.112 keV) and (*e*) the Mn *K*-edge (6.537 keV). (*f*) A visible-light image of the piemontite-quartz schist.

Table 1
Transmission of 7.122 keV X-rays [after Henke *et al.* (1993)].

	Transmission
Be windows (0.7 mm)	0.84
Graphite (0.3 mm)	0.77
Kapton foils (0.24 mm)	0.75
Air path (200 mm)	0.73

crystal monochromator (Ishikawa, 1996) equipped with Si(111) crystals is placed 36 m away from the source. The energy bandwidth ($\Delta E/E$) is $\sim 1 \times 10^{-4}$. Therefore the photon flux through the monochromator is 2.36×10^{16} photons s^{-1} $mrad^{-2}$. The transmission for the incident beam from the source to the sample is shown in Table 1. The incident photon flux density at the sample is $\sim 4.76 \times 10^{12}$ photons s^{-1} mm^{-2} for 7.122 keV X-rays. The excitation efficiency of Fe is shown in Table 2. When these incident X-rays are irradiated on the Fe wire, the Fe $K\alpha$ fluorescence intensity from the wire is 1.46×10^{10} photons s^{-1} mm^{-2}. The solid angle of the Wolter mirror is 1.41×10^{-5} sr, the reflectivity of the mirror is 0.84, and the detection efficiency of the CCD camera is $\sim$0.08 (Tsunemi, 1990). The absorption factors from the sample to the CCD camera are 0.71 (Mylar foils 0.19 mm) and 0.89 (air path 50 mm). Considering all the above factors, the Fe $K\alpha$ fluorescence intensity from the Fe wire on the focal point is calculated to be 0.96 photons s^{-1} $pixel^{-1}$.

Second, the Fe $K\alpha$ fluorescence X-ray intensity from the Fe wire is estimated from the CCD data after irradiation with incident X-rays of energy 7.122 keV. Fig. 6 shows an X-ray fluorescence image of the test specimens and the intensity profile of the Fe wire at an excitation energy of 7.122 keV. The exposure time is 3 min. The binning size of the pixel is 4, the gain of the CCD is low, *i.e.* there are 25 electrons to 1 count. From the profile, the count, which is obtained by subtracting the background, is $\sim$1650. On the CCD (TI, TC215) camera, the number of electrons (N) generated by an incident X-ray photon whose energy is E_{in} is given by

$$N = E_{in}/E_{Si},$$

where E_{Si} is the bandgap of Si (3.65 eV). The number of electrons generated by an Fe $K\alpha$ X-ray photon is 1753. The

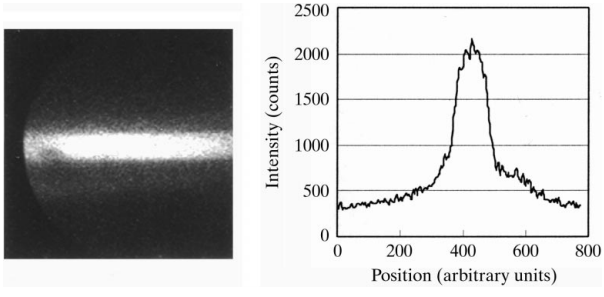

Figure 6
Fe $K\alpha$ fluorescence X-ray image from the Fe wire of diameter 100 μm and its profile at an excitation energy of 7.122 keV.

Table 2
Excitation efficiency of Fe (K series, % indication) [after Birks (1963)].

Energy of incidence X-ray (keV)	Excitation efficiency
10.33	17.0
8.98 (K-edge)	
8.85	19.5
8.38 (K-edge)	
7.75 (K-edge)	21.0
7.12 (K-edge)	22.0

absorption factors for Fe $K\alpha$ fluorescence X-rays from the sample to the CCD camera are 0.71 and 0.89. Taking all of these into consideration, the Fe $K\alpha$ fluorescence X-ray intensity from the Fe wire of diameter 100 μm is 1.0×10^{-1} photons s^{-1} $pixel^{-1}$.

The value derived from the calculation is one order larger than that from the experimental data. Because the monochromator was not yet perfect, the intensity of the incident X-rays was $\sim$0.75 lower than the expected value (Goto *et al.*, 1997; Goto, 1999). Also, the reflectivity of the Fe $K\alpha$ fluorescence X-rays is less than half of the ideal value owing to the slope error of the mirror. Taking these factors into consideration, the Fe $K\alpha$ fluorescence intensity from the Fe wire is about one order smaller than 0.96 photons s^{-1} $pixel^{-1}$, which means that the value calculated from the experimental data is reasonable.

Next, the minimum detection limit (MDL) of this experiment is estimated. The standard deviation (σ) of the background of the subtracted image (see Fig. 3*i*) in 3 min is 1.8 counts; thus the MDL, defined as 3σ, is 5.4 counts (IUPAC, 1976).

The relation between the count and the iron weight is derived from the Fe $K\alpha$ fluorescence X-ray intensity generated from the Fe wire of diameter 100 μm. From the intensity profile in Fig. 3(*i*), the maximum value from which the background value was subtracted is 1150 counts $pixel^{-1}$.

The weight of iron which contributed to an Fe $K\alpha$ fluorescence X-ray intensity of one pixel is estimated. First, the volume of iron is defined. In this optical system the binning size of the pixel is 4 and the magnification of the Wolter mirror is 13; thus the size of pixel on the sample plane is ~ 13.6 μm^2. The penetration depth of iron at energy 7.122 keV is 3.1 μm. As the absorption of the Fe $K\alpha$ fluorescence X-rays through iron of thickness 3.1 μm is almost zero, the effective volume of the iron is 42.1 μm^3. Assuming that the iron wire is pure (density 7.87 g cm^3), the weight of the iron which contributed to an Fe $K\alpha$ fluorescence X-ray intensity (1150 counts) of one pixel is 331.3 pg. Thus a weight of 288.1 fg per count was found, and therefore the MDL is 1.6 pg.

In conclusion, by using the energy of the absorption edge as an excitation monochromatic X-ray, two-dimensional element images of the test specimens and the rock specimen were obtained.

We greatly thank Professor T. Miyano for offering the specimen (a piemontite-quartz schist) and for valuable information on the specimen. This work was partially supported by the Grants-in-Aid for Scientific Research No. 11305011 from the Ministry of Education, Science, Sports, and Culture of Japan.

References

Aoki, S., Takeuchi, A. & Ando, M. (1998). *J. Synchrotron Rad.* **5**, 1117–1118.

Aoki, S., Takeuchi, A., Sakurai, K., Kameno, H., Saito, D., Takano, H., Yamamoto, K., Watanabe, N., Ando, M., Yoshidomi, Y., Shinada, K. & Kato, T. (1997). *J. Phys. IV France*, **7**(C2), 329–330.

Bilderback, D. H., Hoffman, S. A. & Thiel, D. J. (1994). *Science*, **263**, 201–203.

Birks, L. S. (1963). *Electron Probe Microanalysis.* New York: Interscience.

Deer, W. A., Howie, R. A. & Zussman, J. (1975). *Textbook of Rock Forming Minerals*, 8th ed. London: Longman.

Eng, P. J., Newville, M., Rivers, M. L. & Sutton, S. R. (1998). *Proc. SPIE*, **2856**, 36–47.

Goto, S. (1999). Private communication.

Goto, S., Kawamura, N. & Suzuki, M. (1997). *SPring-8 Annual Report 1996*, pp. 88–90. SPring-8, Kamigori, Hyogo 678–12, Japan.

Henke, B. L., Gullikson, E. M. & Davis, J. C. (1993). *X-ray Interact.* **54**, 181–342.

Ishikawa, T. (1996). *SPring-8 Annual Report 1996*, pp. 30–32. SPring-8, Kamigori, Hyogo 678–12, Japan.

IUPAC (1976). *Pure Appl. Chem.* **45**, 99–104.

Kitamura, H. (1994). *SPring-8 Annual Report 1994*, pp. 47–51. SPring-8, Kamigori, Hyogo 678–12, Japan.

Kitamura, H. (1998). *J. Synchrotron Rad.* **5**, 184–188.

Snigireva, A. A., Snigirev, I. I., Bosecke, P., Lequien, S. & Schelokov, I. (1997). *Opt. Commun.* **135**, 378–384.

Suzuki, Y., Kamijyo, N., Tamura, S., Hanada, K., Takeuchi, A., Yamamoto, S., Sugiyama, S., Ohsumi, K. & Ando, M. (1997). *J. Synchrotron Rad.* **4**, 60–63.

Tsunemi, H. (1990). *Oyo Butsuri*, **62**, 718–719.

Yun, W., Lai, B., Krasnoperova, A. A., Fabrizio, E. Di., Cai, Z., Cerrina, F., Chen, Z., Gentili, M. & Gluskin, E. (1999). *Rev. Sci. Instrum.* **70**, 3537–3541.